

The Diffusion Fish

Gunnar Peng

October 15, 2015

1 Introduction

The study of stratified fluids, i.e. bodies of e.g. water or air in which density varies with height, is of great importance for the understanding of the oceans and the atmosphere. As is well known, a system with dense fluid overlying light fluid is unstable, and if left to evolve will spontaneously generate a flow that interchanges and mixes the fluids until a stable stratification is reached, where the density decreases with increasing height. A less well-known fact is that flow can also be spontaneously generated in a stably stratified fluid, and that is the focus of this report. The spontaneous flow is called diffusion-driven flow, and is due to a combination of diffusion and buoyancy effects.

For simplicity, in this report we consider a liquid whose density varies due to a varying concentration of salt, although the discussion applies to thermal stratifications as well. (If the stratification is due to a combination of multiple salts and/or heat with different diffusive properties, then double-diffusive effects may come into play and we do not consider this case here.) In a stable stratification, salt will spontaneously diffuse up from the salty and dense fluid below to the fresh and light fluid above. This raises the centre of gravity of the fluid, and hence increases the potential energy of the system (at the expense of thermodynamic free energy), which can then be harnessed to drive a flow.

The classical example of diffusion-driven flow due to the presence of sloping insulating boundaries was described by Phillips [13] and Wunsch [18] in 1970 (see figure 1(a)). We assume that the stable background stratification is uniform, so that salt diffuses upward at a constant rate. Thus, away from the wall, at each point (e.g. A in the figure) the amount of salt leaving upward due to diffusion equals the amount of salt arriving from below, and hence the concentration does not change. Just above the wall (e.g. B in the figure), however, the salt that diffuses up and away is not replenished from below due to the presence of the insulating wall, and hence (in the absence of flow) the fluid near the wall becomes lighter. Put another way, the pycnoclines (surfaces of constant density) must meet the insulating wall at right angles, and do so by bending down, as shown in the figure, resulting in the fluid near the wall becoming lighter.

The lighter fluid wants to rise (relative to the ambient fluid away from the wall), and hence flows up along the boundary in a “buoyancy layer”. A steady flow is achieved with the velocity profile shown, and the salt leaving point B by diffusion is continually replenished by advection from below (the dashed arrow). Similarly, fluid near a sloping upper boundary becomes heavy, and hence flows down the slope. This buoyancy-layer flow is called Phillips–Wunsch flow, and will be discussed more quantitatively in §2.2.

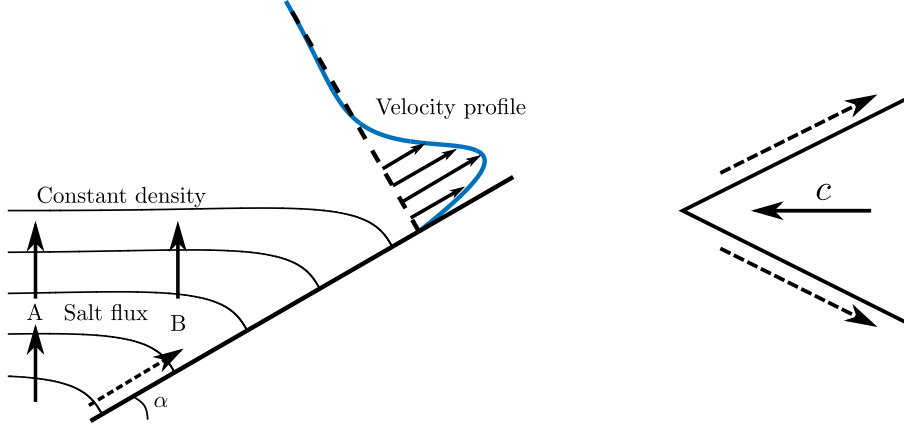


Figure 1: (a) Schematic of diffusion-driven (Phillips–Wunsch) flow near a sloping insulating boundary in stably stratified fluid (adapted from [13, 12]). (b) Schematic of diffusion-driven propulsion. The Phillips–Wunsch flow (dashed arrows) along the sloping surfaces propels the wedge in the opposite direction.

More recent studies of Phillips–Wunsch flow include an experimental verification by Peacock, Stocker and Aristoff in 2004 [12] and a few years later theoretical and numerical studies of the diffusion-driven flow inside containers with sloping walls by Page & Johnson [10, 11] and Page [8, 9].

Around the same time as the original papers by Phillips and Wunsch, the motion of bodies through stably stratified fluids was extensively studied. The existence of an exact analogy between the governing equations for two-dimensional viscous stratified flow and two-dimensional viscous rotating flow (see e.g. Veronis [15, 16, 17]) led to parallel developments in both fields, such as the calculation of the drag on a body moving horizontally in stratified fluid (Foster & Saffman [2]) and axially in a rotating fluid (Moore & Saffman [6, 7]).

Although the Phillips–Wunsch flow on sloping boundaries and the motion of insulating bodies through stratified fluid were thoroughly studied around 1970, these two ideas were not combined until 2010, when Allshouse, Barad and Peacock [1] showed that the Phillips–Wunsch flow could be harnessed by asymmetric bodies for horizontal propulsion. They placed a wedge in stably stratified fluid and found that it moves (see figure 1(b)) at a constant speed c which depends on the parameters of the problem. No studies so far have given a theoretical explanation for the propulsion or prediction for the propulsion speed. We will do so for a variety of two-dimensional cases in this report.

In §2, we describe the assumptions and approximations made and derive the main governing equations. We then investigate three main cases, where the wedge is placed in either a box with insulating walls (§3), a box with fixed-buoyancy walls (§4), or a large or infinite box (§5). Finally, we summarize our results in §6 and discuss possible extensions to this work.

2 Problem Setup

We consider a fluid with constant dynamic viscosity μ , whose density ρ depends on the salinity $S(\mathbf{x}, t)$. We assume that the variations in S about a constant reference value S_0 are sufficiently small that the equation of state can be linearized, i.e.

$$\rho = \rho_0(1 + \beta_S(S - S_0)), \quad (2.1)$$

where β_S is the coefficient of saline contraction and ρ_0 is the reference value for ρ . The (upward) buoyancy force can then be written as

$$-\rho g = \rho_0(-g + B), \quad (2.2)$$

where g is the gravitational acceleration and we have defined the buoyancy (or reduced gravity) by

$$B = g \frac{\rho - \rho_0}{\rho_0} = g\beta_S(S_0 - S). \quad (2.3)$$

The salt is advected by the velocity field $\mathbf{u}(\mathbf{x}, t)$ and diffuses with diffusivity κ , leading to the equation

$$\dot{S} + \mathbf{u} \cdot \nabla S = \kappa \nabla^2 S \quad \Rightarrow \quad \dot{B} + \mathbf{u} \cdot \nabla B = \kappa \nabla^2 B, \quad (2.4a,b)$$

where overdot denotes the time derivative and ∇ is the gradient operator.

We further assume that the Boussinesq approximation holds, so we can ignore any effects due to density variations, apart from the buoyancy force. We thus obtain the incompressible Navier–Stokes equations

$$\rho_0(\dot{\mathbf{u}} + \mathbf{u} \cdot \nabla \mathbf{u}) = -\nabla P + \mu \nabla^2 \mathbf{u} + \rho_0(-g + B) \mathbf{e}_z, \quad \nabla \cdot \mathbf{u} = 0, \quad (2.5a,b)$$

where $P(\mathbf{x}, t)$ is the pressure and \mathbf{e}_z is the unit vector in the vertical direction. As the kinematic viscosity $\nu = \mu/\rho_0$ of the salt solution is much larger than the diffusivity κ of the salt (the Schmidt number is typically $\nu/\kappa \sim 10^3$), the inertial terms (left-hand side) of equation (2.5a) can be neglected for diffusion-driven flow. (We confirm this claim in §2.2.) We are left with the Stokes equations

$$\mathbf{0} = -\nabla(P/\rho_0 + gz) + \nu \nabla^2 \mathbf{u} + B \mathbf{e}_z, \quad \nabla \cdot \mathbf{u} = 0. \quad (2.6a,b)$$

We will solve the main governing equations (2.4b, 2.6) in a domain between the wedge and an outer bounding box, and require boundary conditions on \mathbf{u} and B . As the boundaries are rigid, the fluid satisfies the no-slip condition

$$\mathbf{u} = \mathbf{U}_b, \quad (2.7)$$

where \mathbf{U}_b is the velocity of the boundary. For the buoyancy, we consider either insulating conditions or fixed-buoyancy conditions

$$B_n = 0 \quad \text{or} \quad B = B_b, \quad (2.8)$$

where the subscript n denotes the derivative in the normal direction pointing into the fluid and B_b is the prescribed value. We specify the detailed geometry and choice of condition (2.8) in each separate section.

2.1 Two-dimensional governing equations

We consider the case when the wedge is sufficiently wide (in the y -direction) that the flow can be approximated as being two-dimensional in the x - and z -directions with no variation in the y -direction. This allows introduction of the stream function $\psi(x, z, t)$, defined by $\mathbf{u} = (u, w) = (\psi_z, -\psi_x)$, where subscripts denote differentiation and we omit the y -component of any vector. Incompressibility (2.6b) is then automatically satisfied, while taking the curl of the momentum equation (2.6a) yields the vorticity equation

$$B_x = \nu \nabla^4 \psi, \quad (2.9a)$$

which describes a balance between the generation of vorticity $\nabla^2 \psi$ by horizontal variations in buoyancy and the dissipation of vorticity by viscous effects. The advection–diffusion equation takes the form

$$\dot{B} + \psi_z B_x - \psi_x B_z = \kappa \nabla^2 B. \quad (2.9b)$$

We consider mainly the case when the buoyancy field has a uniform background stratification $N^2 z$, and the perturbations $b = B - N^2 z$ to the buoyancy field are small compared with the background. The gradient N^2 of the background field is the square of the Brunt–Väisälä (buoyancy) frequency. After the change of variables from B to b , the governing equations (2.9) become

$$b_x = \nu \nabla^4 \psi, \quad \dot{b} + \psi_z b_x - \psi_x b_z - N^2 \psi_x = \kappa \nabla^2 b. \quad (2.10a,b)$$

Typically, the term $-N^2 \psi_x$ in (2.10b), which expresses advection of the background stratification N^2 by the vertical velocity $-\psi_x$, dominates the remaining terms on the left-hand side. In this case, we can eliminate either ψ or b from (2.10) to obtain

$$b_{xx} + \frac{\kappa \nu}{N^2} \nabla^6 b = 0 \quad \text{or} \quad \psi_{xx} + \frac{\kappa \nu}{N^2} \nabla^6 \psi = 0. \quad (2.11)$$

This reveals an inherent length scale

$$L_0 = \left(\frac{\kappa \nu}{N^2} \right)^{1/4} \quad (2.12)$$

of the governing equations. The equations (2.10) or (2.11) are typically too complicated to solve exactly, so we will restrict ourselves to cases where the other length scales of the problem (such as the size of the wedge and the size of the domain) are much larger than L_0 , and use the method of matched asymptotic expansions to obtain approximate analytical solutions.

Although equations (2.10) suffice to describe the flow and buoyancy fields, we will need the pressure in order to calculate the force on the wedge. Hence, we retain the momentum equation (2.6a) as well, in the form

$$p_x = \nu(\psi_{zxx} + \psi_{zzz}), \quad p_z = -\nu(\psi_{xxx} + \psi_{xzz}) + b, \quad (2.13)$$

where we have defined the rescaled pressure perturbation $p = P/\rho_0 + gz - N^2 z^2/2$.

2.2 Solutions near non-horizontal walls

As discussed in the introduction, diffusion-driven flow is generated by the interaction of stratified fluid with sloping boundaries. We investigate the details of this in more detail, by considering an infinite wall with angle α to the horizontal placed in a stratified fluid with linear ambient stratification $B = N^2 z$ and no ambient flow (see figure 1(a)). The solutions obtained here will serve as boundary-layer solutions for later calculations, and so the aim in particular is to understand the far-field behaviour of these solutions.

We seek steady solutions for the buoyancy perturbation b and the stream function ψ which depend only on the distance η from the wall, and hence are independent of the distance along the wall. The governing equations (2.10) reduce to

$$-\sin \alpha b_\eta = \nu \psi_{\eta\eta\eta\eta}, \quad N^2 \sin \alpha \psi_\eta = \kappa b_{\eta\eta}. \quad (2.14)$$

As the wall is stationary, the no-slip condition (2.7) yields

$$\psi = 0, \quad \psi_\eta = 0 \quad \text{at } \eta = 0, \quad (2.15)$$

where we have chosen the arbitrary additive constant for the stream function such that $\psi = 0$ on the wall.

If the wall is insulating (which is the case for Phillips–Wunsch flow), then the condition (2.8) for no perpendicular gradient of total buoyancy $B = N^2 z + b$ yields

$$b_\eta = -N^2 \cos \alpha \quad \text{at } \eta = 0. \quad (2.16)$$

The solution to equations (2.14, 2.15, 2.16) that does not grow exponentially as $\eta \rightarrow \infty$ is

$$\psi = \kappa \cot \alpha [1 - (\cos \gamma \eta + \sin \gamma \eta) e^{-\gamma \eta}], \quad b = N^2 \frac{\cos \alpha}{\gamma} \cos \gamma \eta e^{-\gamma \eta} + b_\infty, \quad (2.17)$$

where b_∞ is a constant of integration and

$$\gamma^{-1} = \left(\frac{4\kappa\nu}{N^2 \sin^2 \alpha} \right)^{1/4} = \sqrt{\frac{2}{\sin \alpha}} L_0 \quad (2.18)$$

is the length scale on which the flow decays away from the wall. We conclude that there is a flow confined to a boundary layer of thickness $O(L_0)$ near the wall, and the net flux of fluid up the slope is the far-field value $\kappa \cot \alpha$ of the stream function ψ . Although in this case we would set the constant of integration b_∞ to be zero, to recover the ambient stratification with $b \rightarrow 0$ as $\eta \rightarrow \infty$, we note that this is in general not necessary and the far-field buoyancy perturbation could have a non-zero value.

We note that the Phillips–Wunsch flux $\kappa \cot \alpha$ is zero for vertical walls ($\alpha = \pi/2$). In this case, the solution is in fact trivial ($\psi = 0$, $b = b_\infty$) and there is no boundary-layer flow. As the slope α decreases, the flux increases and eventually diverges to infinity as α approaches zero and the wall becomes horizontal. We thus assume for the rest of this report that α is not too small, so that $\cot \alpha = O(1)$. In our analyses that follow, the velocity is largest in the Phillips–Wunsch boundary layer, so the Reynolds number is everywhere smaller than the local estimate $\kappa \cot \alpha / \nu$. Since $\nu \gg \kappa$, the use of the Stokes equations (2.6) is indeed appropriate.

If instead the wall has prescribed buoyancy (i.e. salinity) $B = N^2 z$, then

$$b = 0 \quad \text{at } \eta = 0, \quad (2.19)$$

and the solution to (2.14, 2.15, 2.19) that does not grow exponentially as $\eta \rightarrow \infty$ is

$$\psi = -\frac{\kappa b_\infty}{N^2} \frac{\gamma}{\sin \alpha} [1 - (\cos \gamma \eta + \sin \gamma \eta) e^{-\gamma \eta}], \quad b = b_\infty [1 - \cos \gamma \eta e^{-\gamma \eta}] \quad (2.20)$$

This result states that the difference b_∞ in buoyancy between the far field and the wall drives a flux proportional to b_∞ in an $O(L_0)$ boundary layer near the wall.

3 Wedge in a Box with Insulating Walls

We first consider the case when the wedge is placed in a box with insulating walls. On the top and bottom of the box, we assume that the buoyancy is held fixed at two different constant values, which would generate a uniform stable stratification $B = N^2 z$ in the absence of a wedge.

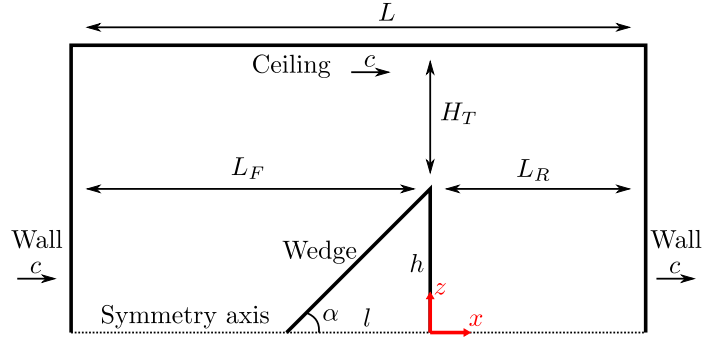


Figure 2: Schematic geometry for a wedge placed inside a box.

The wedge is placed with its apex pointing to the left (see figure 2), which turns out to be its direction of motion. We work in the frame of reference moving with the wedge, with the origin $(0, 0)$ at the midpoint of the back of the wedge at all times. We assume that the level of neutral buoyancy of the wedge is vertically centred in the box, and that the initial conditions are symmetric about $z = 0$. Hence, the top-down symmetry will be preserved throughout the evolution, and we need only consider the upper half $z \geq 0$ of the system.

The wedge has length l and (half-)height h , so that its corners are at $(-l, 0)$ and $(0, h)$. Its apex half-angle is α , so that

$$\cot \alpha = \frac{l}{h}. \quad (3.1)$$

The box has length $L = L_F + L_R$, where $L_F(t)$ and $L_R(t)$ are the distances from the front (left) wall and the rear (right) wall to the base of the wedge and evolve according to

$$c = -\dot{L}_F = \dot{L}_R, \quad (3.2)$$

where $c(t)$ is the leftward speed of the wedge (and hence, in this reference frame, the rightward speed of the bounding box). The height of (the upper half of) the box is $h + H_T$.

We assume that the wedge has a length scale L_1 which is much greater than the natural scale L_0 of the flow given in (2.12). (In the experiments [1], typically $L_1 = O(10 \text{ mm})$ and $L_0 = O(0.1 \text{ mm})$.) We thus obtain a small parameter

$$\varepsilon = L_0/L_1 \quad (3.3)$$

that we can exploit using the method of matched asymptotic expansions. We also take the height H_T of the box to be $O(L_1)$, but in this section we assume that the horizontal dimensions L_F and L_R of the box are $O(\varepsilon^{-1}L_1)$, i.e. much larger than the dimensions of the wedge.

At every instant in time, we seek to calculate the flow field (via the stream function $\psi(x, z, t)$), the buoyancy distribution $b(x, z, t)$, and the net ‘‘propulsive’’ left-ward force $F(t)$ on (the upper half of) the wedge as a function of the unknown speed $c(t)$ of the wedge. Requiring that $F = 0$ then determines the actual value $c(t)$.

We non-dimensionalize the variables as follows. Length is scaled by L_1 , except for L_F and L_R which are scaled by $\varepsilon^{-1}L_1$. Given that the flow is driven by the Phillips–Wunsch flux $\kappa \cot \alpha$ (see §2.2), we scale the stream function by κ and velocity by κ/L_1 . We scale time by $\varepsilon^{-1}L_1^2/\kappa$, as this is the time scale of the overall evolution due to the horizontal motion of the wedge. (We neglect the fast initial adjustment at the start of the experiment.) Buoyancy perturbations are scaled by $\varepsilon N^2 L_1$, for reasons which will become clear later (and thus we scale the pressure and force by $\varepsilon N^2 L_1^2$ and $\varepsilon N^2 L_1^3$ respectively). The rescaled governing equations (2.10) are thus

$$b_x = \varepsilon^3 \nabla^4 \psi, \quad \varepsilon^2 \dot{b} + \varepsilon(\psi_z b_x - \psi_x b_z) - \psi_x = \varepsilon \nabla^2 b. \quad (3.4a,b)$$

We choose the stream function ψ to be zero on the centreline $z = 0$. Hence, ψ (as well as b) are odd functions of z , and we obtain the symmetry conditions

$$\psi = \psi_{zz} = 0, \quad b = 0 \quad \text{on symmetry axis} \quad z = 0. \quad (3.5a)$$

The boundary conditions on the insulating wedge (analogous to (2.16)) are

$$\psi = \psi_n = 0, \quad b_n = -\frac{1}{\varepsilon} \cos \alpha \quad \text{on wedge front} \quad x = -l + z \cot \alpha, \quad (3.5b)$$

$$\psi = \psi_n = 0, \quad b_n = 0 \quad \text{on wedge rear} \quad x = 0. \quad (3.5c)$$

On the bounding box, which moves to the right at speed $c(t)$, we have the no-slip condition and insulating or prescribed-buoyancy conditions:

$$\psi = cz, \quad \psi_x = 0, \quad b_x = 0 \quad \text{on walls} \quad x = -\varepsilon^{-1}L_F, \varepsilon^{-1}L_R, \quad (3.5d)$$

$$\psi = cz, \quad \psi_z = c, \quad b = 0 \quad \text{on ceiling} \quad z = h + H_T. \quad (3.5e)$$

For a given value of $c(t)$, ψ and b are determined uniquely by the equations (3.4) and boundary conditions (3.5). Equation (2.13), which in non-dimensional form is

$$p_x = \varepsilon^3(\psi_{zxx} + \psi_{zzz}), \quad p_z = -\varepsilon^3(\psi_{xxx} + \psi_{xzz}) + b, \quad (3.6a,b)$$

then determines the pressure up to an arbitrary additive constant, which we can choose without loss of generality such that $p = 0$ at $(x, z) = (0, h + H_T)$. The horizontal leftward force on the wedge is given by

$$F(t) = \int_0^h [(-p + \varepsilon^3 2\psi_{xz}) + \varepsilon^3(\psi_{xx} - \psi_{zz}) \cot \alpha]_{x=-l+z \cot \alpha} + [p - \varepsilon^3 2\psi_{xz}]_{x=0} dz, \quad (3.7)$$

and the correct value of $c(t)$ is the one that makes $F(t)$ vanish.

3.1 Numerical results using the finite-element method

In order to inform, and later validate, our asymptotic analysis, we developed a simple code in FreeFem++ [4] that solves the governing equations (3.4, 3.5). However, for simplicity we do not simulate the full time-evolution of the system with moving boundaries. Instead, we neglect the time derivative \dot{b} in (3.4b), as it is of higher order than the other terms. This quasi-static approximation leaves us with an instantaneous problem with no time derivatives, that is readily solved by our program.

For our numerical calculations, we use the following parameters:

$$\varepsilon = \frac{L_0}{L_1} = \frac{1}{100}, \quad h = H_T = 1, \quad L = 1, \quad (L_F, L_R) = \left(\frac{1}{4}, \frac{3}{4}\right), \left(\frac{1}{2}, \frac{1}{2}\right), \left(\frac{3}{4}, \frac{1}{4}\right), \quad (3.8)$$

with a focus on the symmetric case $L_F = L_R = 1/2$ with $\alpha = 45^\circ$. Figure 3 shows results for this particular case.

We observe that a Phillips–Wunsch boundary layer develops on the sloping surface of the wedge, and that fluid arrives in a boundary layer near $z = 0$ in front of the wedge (to the left), and leaves in a boundary layer near $z = h$ behind the wedge (to the right). The buoyancy perturbations are approximately uniform in x both in front of, behind and above the wedge. As we shall see, the buoyancy field is key to calculating the force on the wedge, and we will show more detailed results later in §3.3.

3.2 Asymptotic calculation

We divide the domain into the regions shown schematically in figure 4(b). The bulk of the fluid is divided into three “outer” regions which we call the front region, the rear region, and the top region. These regions are joined by horizontal boundary layers at $z = h$, and in addition there are boundary layers at $z = 0$.

3.2.1 Boundary layers on the insulating surfaces

Near the sloping surface of the wedge (but away from the corners), we expect to find a boundary layer with the Phillips–Wunsch solution discussed in §2.2. Indeed, if we define rescaled coordinates (η, χ) perpendicular and parallel to the slope by

$$x = -l + \chi \cos \alpha - \varepsilon \eta \sin \alpha, \quad z = \chi \sin \alpha + \varepsilon \eta \cos \alpha, \quad (3.9)$$

then the governing equations (3.4) and boundary conditions (3.5b) on the wedge become

$$-\sin \alpha b_\eta + \varepsilon \cos \alpha b_\chi = b_{\eta\eta\eta} + \varepsilon^2 2b_{\eta\eta\chi} + \varepsilon^4 b_{\chi\chi\chi}, \quad (3.10a)$$

$$\varepsilon^3 \dot{b} + \varepsilon(\psi_\eta b_\chi - \psi_\chi b_\eta) + \sin \alpha \psi_\eta - \varepsilon \cos \alpha \psi_\chi = b_{\eta\eta} + \varepsilon^2 b_{\chi\chi}, \quad (3.10b)$$

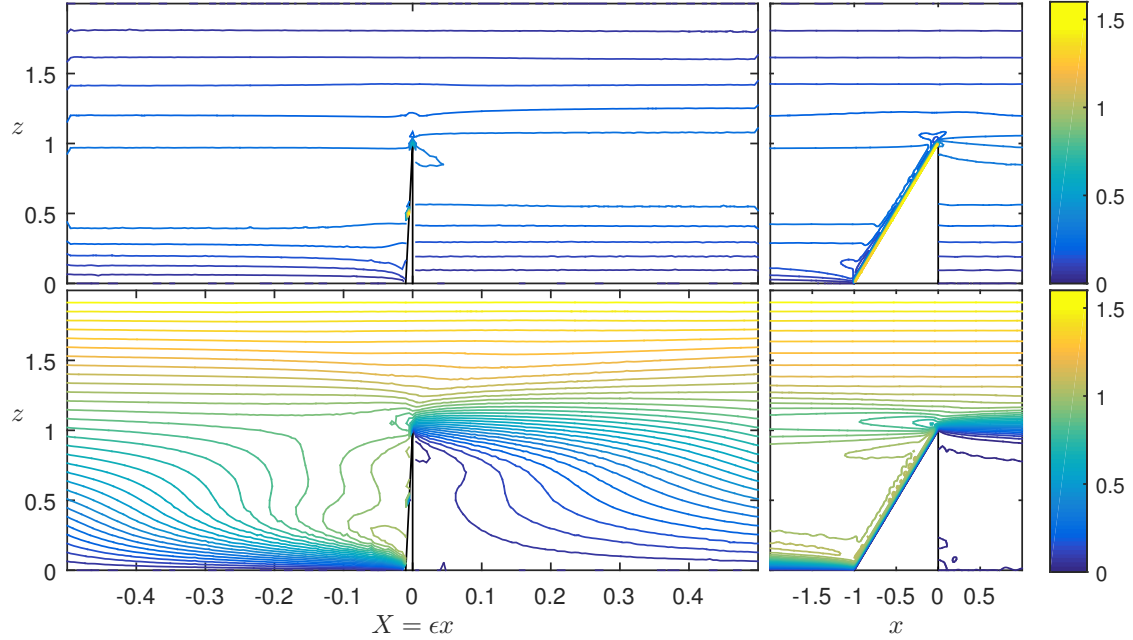


Figure 3: Contour plots of buoyancy perturbation b (top row) and stream function ψ (bottom row, flow from left to right in the frame of reference of the wedge) showing the whole box with stretched coordinates (left) and a close-up of the wedge (right), for the parameters (3.8), $L_F = L_R = 1/2$, $\alpha = 45^\circ$. The contour spacing is 0.05. (The irregularities in the contours are artefacts of the plotting tool and are not present in the original data.)

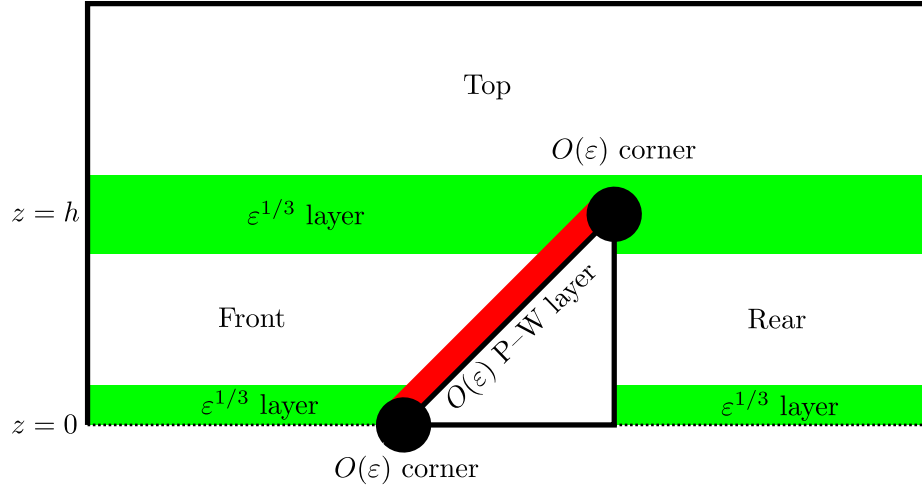


Figure 4: Schematic of asymptotic regions for a wedge in a box with insulating walls.

$$\psi = \psi_\eta = 0, \quad b_\eta = -\cos \alpha \quad \text{on the wedge } \eta = 0. \quad (3.10c)$$

These equations are analogous to the equations (2.14, 2.15, 2.16) for Phillips–Wusch flow at leading order, and hence the solution (which does not grow exponentially as $\eta \rightarrow \infty$) is

$$\psi = \cot \alpha [1 - (\cos \gamma \eta + \sin \gamma \eta) e^{-\gamma \eta}] + O(\varepsilon), \quad (3.11a)$$

$$b = \cot \alpha \sqrt{2 \sin \alpha} \cos \gamma \eta e^{-\gamma \eta} + b_\infty(\chi) + O(\varepsilon), \quad (3.11b)$$

where $\gamma = \sqrt{\sin \alpha / 2}$, analogously to (2.17).

The far-field behaviour of the solution (3.11) is to be matched to the outer solution for the front region. We find that

$$\psi \rightarrow \cot \alpha + O(\varepsilon), \quad b \rightarrow b_\infty(\chi) + O(\varepsilon) \quad \text{as } \eta \rightarrow \infty. \quad (3.12)$$

For the buoyancy field, the matching determines the constant of integration $b_\infty(\chi)$ to be the effective value $b^F(-l + \chi \cos \alpha, \chi \sin \alpha)$ of the outer buoyancy field b^F on the wedge, but imposes no constraint on b^F . However, the outer stream function ψ^F ahead of the wedge must satisfy the effective condition

$$\psi^F = \cot \alpha + O(\varepsilon) \quad \text{on the wedge } x = -l + z \cot \alpha. \quad (3.13a)$$

Since the back of the wedge is vertical, the corresponding boundary layer there is trivial at leading order (as discussed in §2.2). Hence the boundary condition (3.5c) for the stream function on the rear of the wedge becomes the effective condition on the leading-order stream function ψ_0^R in the rear region:

$$\psi^R = 0 + O(\varepsilon) \quad \text{on the wedge } x = 0. \quad (3.13b)$$

The insulating front and rear wall behave like the insulating back of the wedge, and hence also have trivial boundary layers. The conditions (3.5d) on the stream function then translate to effective conditions on the outer solutions, including ψ^T for the top region:

$$\psi^F = cz + O(\varepsilon) \quad \text{at } x = -\varepsilon^{-1} L_F, \quad \psi^R = cz + O(\varepsilon) \quad \text{at } x = \varepsilon^{-1} L_R, \quad (3.13c)$$

$$\psi^T = cz + O(\varepsilon) \quad \text{at } x = -\varepsilon^{-1} L_F, \quad \psi^T = cz + O(\varepsilon) \quad \text{at } x = \varepsilon^{-1} L_R. \quad (3.13d)$$

3.2.2 Outer solution

Using the conditions (3.13), we can now start obtaining solutions for the outer regions. As these regions have length $O(\varepsilon^{-1})$, we introduce a scaled horizontal coordinate $X = \varepsilon x$. The governing equations (3.4) become

$$b_X = \varepsilon^2 (\psi_{zzzz} + \varepsilon^2 \psi_{XXzz} + \varepsilon^4 \psi_{XXXX}), \quad (3.14a)$$

$$\varepsilon (\dot{b} + \psi_z b_X - \psi_X b_z) - \psi_X = b_{zz} + \varepsilon^2 b_{XX}. \quad (3.14b)$$

At leading order, these equations simplify to

$$b_X = 0 + O(\varepsilon), \quad -\psi_X = b_{zz} + O(\varepsilon). \quad (3.15a,b)$$

Equation (3.15a) describes how the flow is too weak to sustain horizontal variations in buoyancy, and thus we obtain $b = b(z, t) + O(\varepsilon)$ in every outer region. Equation (3.15b)

describes how the vertical diffusion of buoyancy is balanced by advection of the background buoyancy field by the vertical velocity $-\psi_X$. By integrating this equation in X , and applying the conditions (3.13), we obtain equations describing the balance of vertical flux in each outer region:

$$L_F b_{zz}^F = \psi^F|_{X=-L_F} - \psi^F|_{X=O(\varepsilon)} + O(\varepsilon) = cz - \cot \alpha + O(\varepsilon), \quad (3.16a)$$

$$L_R b_{zz}^R = \psi^R|_{X=0} - \psi^R|_{X=L_R} + O(\varepsilon) = -cz + O(\varepsilon), \quad (3.16b)$$

$$L b_{zz}^T = \psi^T|_{X=-L_F} - \psi^T|_{X=L_R} + O(\varepsilon) = 0 + O(\varepsilon). \quad (3.16c)$$

We also obtain the stream function directly as

$$\psi_F = -X \frac{cz}{L_F} + \cot \alpha \frac{L_F + X}{L_F} + O(\varepsilon), \quad (3.17a)$$

$$\psi_R = X \frac{cz}{L_R} + O(\varepsilon), \quad (3.17b)$$

$$\psi_T = 0 + O(\varepsilon). \quad (3.17c)$$

The equations (3.16) are ordinary differential equations for $b^{F,R,T}$ depending on the variable z , and require boundary and matching conditions at $z = 0$, h , $h + H_T$. At the ceiling $z = h + H_T$, the condition (3.5e) that b vanishes applies directly. However, the conditions at $z = 0$ and $z = h$ are obtained from consideration of horizontal boundary layers. These calculations are quite complicated and not very enlightening, so we will deal with them later in §3.4.

We assert for now that b is continuous to leading order at the symmetry axis, and in fact

$$b^{F,R} = 0 + O(\varepsilon^{2/3}) \text{ on symmetry axis } z = 0. \quad (3.18)$$

Applying this condition and the ceiling condition yields the results

$$b^F = c \frac{z^3 - h^2 z}{6L_F} - \cot \alpha \frac{z^2 - hz}{2L_F} + A_F \frac{z}{h} + O(\varepsilon^{2/3}), \quad (3.19a)$$

$$b^R = -c \frac{z^3 - h^2 z}{6L_R} + A_R \frac{z}{h} + O(\varepsilon^{2/3}), \quad (3.19b)$$

$$b^T = A_T \frac{h + H_T - z}{H_T} + O(\varepsilon^{2/3}), \quad (3.19c)$$

where $A_{F,R,T}$ are constants of integration to be determined by matching at $z = h$.

At $z = h$, the boundary-layer solutions from §3.4 yield continuity of b at leading order and continuity of the total vertical diffusive buoyancy flux (with $O(\varepsilon^{1/3})$ errors),

$$b^F = b^R = b^T, \quad L_F b_z^F + L_R b_z^R = L b_z^T \quad \text{at } z = h. \quad (3.20a,b)$$

(We note that full continuity of b_z would be two conditions rather than one, and hence too many conditions to impose.) Applying these conditions to the solutions (3.19) determines the constants

$$A_F, A_R, A_T = \cot \alpha \frac{h^2}{2L(1 + h/H_T)} + O(\varepsilon^{1/3}), \quad (3.21)$$

which are substituted back into (3.19) to yield the solution.

3.2.3 Force calculation

Having calculated the stream function and buoyancy field in the main outer regions, we now have sufficient information to determine the leading-order force F on (the upper half of) the wedge. Since forces balance for Stokes flow and no horizontal body forces are present, the net horizontal force from the fluid on the wedge is equal and opposite to the horizontal force from the fluid on the bounding box, which is simpler to calculate.

As we can see from (3.6b), the pressure is approximately hydrostatic, $p_z \approx b$, in the outer region (and it is straightforward to check that this also holds true in the horizontal boundary layers). In addition, the forces on the bounding box are due to pressure only at leading order. Hence, the leading-order force is given by the difference in pressure on the front and rear walls.

As pressure is only defined up to an additive constant, we are free to choose the pressure to be zero at the point $(0, h + H_T)$ on the ceiling directly above the base of the wedge. From (3.6a), we thus find that $p = 0 + O(\varepsilon^3)$ along the top wall. Instead of obtaining the pressure field from separate asymptotic expansions in each region, we make use of the approximate hydrostatic relationship to write

$$p = - \int_z^{h+H_T} b dz + O(\varepsilon), \quad (3.22)$$

and hence the force on either wall is

$$\tilde{F} = \int_0^{h+H_T} p dz + O(\varepsilon) = - \int_0^{h+H_T} b z dz + O(\varepsilon), \quad (3.23)$$

where the latter expression is obtained by using (3.22) and interchanging the order of the two integrals.

The net force is the difference between (3.23) for the front and rear walls. In the top region, the outer solution (3.19c) is independent of X , and hence contributes equally to both integrals and has no effect. The leading-order leftward force on the wedge (rightward force on the wall), obtained from the outer solutions (3.19a,b), is thus

$$F = \int_0^h (b^F - b^R) z dz = \cot \alpha \frac{h^4}{24L_F} - c \frac{h^5}{45} \left(\frac{1}{L_F} + \frac{1}{L_R} \right) + O(\varepsilon^{1/3}). \quad (3.24)$$

The first term, which is proportional to $\cot \alpha$, describes the propulsive force on the wedge due to the diffusion-driven flow. The second term, which is proportional to c , describes the drag on the wedge and was originally calculated by Foster & Saffman [2]. For a free wedge, the two forces balance, and hence the wedge moves at speed

$$c = \frac{\cot \alpha}{h} \frac{15L_R}{8L} + O(\varepsilon^{1/3}). \quad (3.25)$$

(The dimensional version of this result simply has an additional factor κ on the right-hand side.)

Finally, we note that the leading-order result for the speed (3.25) does not depend on the height of the bounding box. In fact, this result also applies for other types of

boundary conditions on the top and bottom surfaces, such as a fixed-flux condition. This is because, although such changes would affect the resulting values of the constants $A_{F,R,T}$, the expression (3.24) for the forces depends on these only through the difference $(A_F - A_R)$, which is always prescribed by the matching condition (3.20) to be zero at leading order.

3.3 Summary and comparison between asymptotic and numerical results

Our asymptotic analysis has revealed the physical mechanisms behind diffusion-driven propulsion: The sloping surface of the wedge induces a Phillips–Wunsch flow up the slope. For a stationary wedge, this flux is balanced by a uniform downwelling in the front region with the same flux, which advects buoyant liquid downward and hence reduces the hydrostatic pressure in front of the wedge. The pressure difference between the front and the rear regions results in a leftward propulsive force. When the wedge moves forward, the downwelling is reduced since part of the fluid volume removed by the Phillips–Wunsch flux is balanced by the front region shrinking instead. A force-free wedge moves at the speed (3.25), for which the net force is zero.

Figure 5(a) shows a comparison between the asymptotically predicted and numerically calculated buoyancy profiles (using the same parameters as in §3.1). We find that there is good agreement between the two, confirming the validity of the asymptotic analysis. Figure 5(b) shows the dependence of the propulsion speed c on the slope of the wedge and the distances L_F and L_R to the front and rear walls. Again, a good agreement is achieved between the asymptotic and numerical results. (Also shown are a set of results calculated in §3.4, which include $O(\varepsilon^{1/3})$ corrections to the leading-order result calculated so far.)

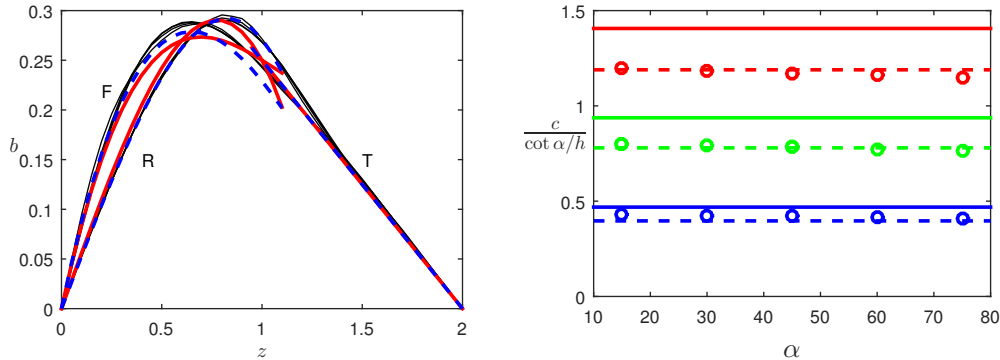


Figure 5: Comparison between asymptotic and numerical results. (a) Buoyancy distribution b as a function of vertical position z for the case shown in figure 3. The thin black curves are numerical data from vertical slices $X = \pm 0.1, \pm 0.2, \pm 0.3, \pm 0.4$ in the forward and rear regions. The thick curves are asymptotic results (3.19), with the leading-order coefficients (3.21, 3.25) (solid red curves) or the corrected ones (3.41, 3.43) below (dashed blue curves). (b) Propulsion speed c as a function of wedge slope α for the parameters (3.8), showing numerical results (circles), leading-order asymptotic results (3.25) (solid lines) and corrected asymptotic results (3.43) below (dashed lines). The values of (L_F, L_R) are $(1/4, 3/4)$ (top red series), $(1/2, 1/2)$ (middle green series) and $(3/4, 1/4)$ (bottom blue series).

The reason for choosing to work with a large, i.e. $O(\varepsilon^{-1}L_1)$, bounding box is now clear:

The upward Phillips–Wunsch flux, which in dimensional terms is $O(\kappa)$, is balanced by a downwelling with velocity $O(\kappa/L_F)$ in the forward region. The resulting advective flux of buoyancy $O(N^2 L_1 \kappa/L_F)$ is in turn balanced by diffusion of the buoyancy perturbations, which must be $b = O(N^2 L_1^2/L_F)$. For $L_F \gg L_1$, the buoyancy perturbation is small compared with the background buoyancy $B = O(N^2 L_1)$, and hence the non-linear advective terms and time derivative in the governing equation (2.10b) could be neglected.

If the dimensions of the box are $O(L_1)$, then the buoyancy perturbations are of the same order as the background stratification. In addition, the change in geometry of the system due to the motion of the wedge occurs on a faster time scale L_1^2/κ due to the reduced length of the box. Thus, both the time derivative and the non-linear terms become important, and the problem becomes more complicated. However, the mechanism of propulsion and the qualitative flow structure can be expected to remain the same.

3.4 The $\varepsilon^{1/3}$ layers and $O(\varepsilon^{1/3})$ corrections

We complete our analysis by calculating the boundary-layer solutions near $z = 0$ and $z = h$ that will yield the conditions, such as (3.20), asserted earlier in §3.2.2. These calculations are mostly a technicality, which is why we have left them to this separate subsection.

We first deal with the boundary layer near $z = 0$ in the forward region $-L_F < X < O(\varepsilon)$. The scaling $z \sim \varepsilon^{1/3}$ yields a new balance in the governing equations (3.14), so we define the rescaled vertical coordinate $\zeta = z/\varepsilon^{1/3}$. The governing equations (3.14) then become

$$b_X = \varepsilon^{2/3} \psi_{\zeta\zeta\zeta\zeta} + O(\varepsilon^3), \quad -\varepsilon^{2/3} \psi_X = b_{\zeta\zeta} + O(\varepsilon). \quad (3.26)$$

The domain under consideration is (up to $O(\varepsilon)$) an infinite strip $-L_F < X < 0$, $-\infty < \zeta < \infty$. The appropriate effective boundary conditions in the X -direction are obtained by revisiting the calculations for the Phillips–Wunsch boundary-layer solution with a rescaled vertical coordinate ζ :

$$\psi = \varepsilon^{1/3} \zeta + O(\varepsilon^{2/3}) \text{ at } X = -L_F, \quad \psi = \cot \alpha + O(\varepsilon^{2/3}) \text{ at } X = 0. \quad (3.27)$$

In the ζ -direction, we have the symmetry-axis conditions (3.5a) at $\zeta = 0$, and must also match to the outer solution as $\zeta \rightarrow \infty$.

We assume that the outer solution has an expansion

$$b^F = b_0^F + \varepsilon^{1/3} b_1^F + \varepsilon^{2/3} b_2^F + O(\varepsilon) \quad (3.28a)$$

with the generic behaviour (for $i = 0, 1, 2$)

$$b_i^F = C_i^F + D_i^F z + E_i^F z^2 + O(z^3) \quad \text{as } z \rightarrow 0. \quad (3.28b)$$

We expand the boundary-layer solution as

$$b = b_0 + \varepsilon^{1/3} b_1 + \varepsilon^{2/3} b_2 + O(\varepsilon), \quad \psi = \psi_2 + O(\varepsilon^{1/3}), \quad (3.29a)$$

and find that matching to the outer solutions (3.28b) requires

$$b_0 \sim C_0^F, \quad b_1 \sim C_1^F + D_0 \zeta, \quad b_2 \sim C_2^F + D_1 \zeta + E_0 \zeta^2 \quad \text{as } \zeta \rightarrow \infty. \quad (3.29b)$$

(It is straightforward to verify a posteriori that a correct matching of b also yields the correct matching of ψ , so we do not consider the latter here.)

At $O(1)$ and $O(\varepsilon^{1/3})$, the governing equations (3.26) yield that b_0 and b_1 are linear functions of ζ . Imposing the matching conditions (3.29b) and symmetry-axis conditions (3.5a) yields

$$b_0 = 0, \quad b_1 = D_0\zeta, \quad C_0^F = C_1^F = 0. \quad (3.30)$$

This confirms the condition (3.18) for the forward region, and the same analysis applies to the rear region as well.

The adjustment of ψ from a non-zero value (3.17a) in the outer solution to zero on the symmetry axis (3.5a) occurs here at $O(\varepsilon^{2/3})$. The equations

$$b_{2X} = \psi_{2\zeta\zeta\zeta\zeta}, \quad -\psi_{2X} = b_{2\zeta\zeta}, \quad (3.31a,b)$$

are to be solved with boundary conditions (3.5a), (3.27) and (3.29b). A solution can be found using e.g. Fourier transforms and yields a condition on C_2 (i.e. the value of the outer solution b^F on the symmetry axis at $O(\varepsilon^{2/3})$), but we do not present this here.

Instead, we turn to the boundary layer near $z = h$, for which we define the rescaled coordinate $\zeta = (z - h)/\varepsilon^{1/3}$. In addition, it turns out that the stream function must be $O(\varepsilon^{-1/3})$ to deal with leading-order differences in b_z , so we define a rescaled stream function $\Psi = \varepsilon^{1/3}\psi = O(1)$. We follow the same steps as for the boundary layer at $z = 0$, but the analysis is more complicated.

The rescaled governing equations are

$$b_X = \varepsilon^{1/3}\Psi_{\zeta\zeta\zeta\zeta} + O(\varepsilon^3), \quad -\varepsilon^{1/3}\Psi_X = b_{\zeta\zeta} + O(\varepsilon), \quad (3.32)$$

and the domain is again an infinite strip $-L_F < X < L_R$, $-\infty < \zeta < \infty$ but with a cut at $X = 0$, $-\infty < \zeta \leq 0$ representing the wedge whose thickness $X = O(\varepsilon^{4/3})$ can be neglected at leading order. The appropriate boundary conditions in the X -direction are

$$\Psi = \varepsilon^{1/3}ch + O(\varepsilon^{2/3}) \quad \text{on walls} \quad X = -L_F, L_R, \quad -\infty < \zeta < \infty \quad (3.33a)$$

$$\Psi = \varepsilon^{1/3} \cot \alpha + O(\varepsilon^{2/3}) \quad \text{on wedge} \quad X = 0^-, \quad \zeta < 0 \quad (3.33b)$$

$$\Psi = 0 + O(\varepsilon^{2/3}) \quad \text{on wedge} \quad X = 0^+, \quad \zeta < 0. \quad (3.33c)$$

We expand the outer solutions as

$$b^{F,R,T} = b_0^{F,R,T} + \varepsilon^{1/3}b_1^{F,R,T} + \varepsilon^{2/3}b_2^{F,R,T} + O(\varepsilon), \quad (3.34a)$$

$$b_i^{F,R,T} = C_i^{F,R,T} + D_i^{F,R,T}(z - h) + E_i^{F,R,T}(z - h)^2 + O(z - h)^3 \quad \text{as } z \rightarrow h, \quad (3.34b)$$

and expand the boundary-layer solution as

$$b = b_0 + \varepsilon^{1/3}b_1 + \varepsilon^{2/3}b_2 + O(\varepsilon), \quad \Psi = \Psi_1 + \varepsilon^{1/3}\Psi_2 + O(\varepsilon). \quad (3.35a)$$

The resulting matching conditions are

$$b_0 \sim C_0^{F,R,T}, \quad (3.35b)$$

$$b_1 \sim C_1^{F,R,T} + D_0^{F,R,T}\zeta, \quad (3.35c)$$

$$b_2 \sim C_2^{F,R,T} + D_1^{F,R,T}\zeta + E_0^{F,R,T}\zeta^2, \quad (3.35d)$$

as $|\zeta| \rightarrow \infty$ in each corresponding region.

At leading order, the governing equations (3.32) reveal that b_0 is a linear function of ζ , but the matching conditions (3.35b) prevent b_0 from growing linearly with ζ , so

$$b_0 = \text{constant} = C_0^F = C_0^R = C_0^T. \quad (3.36)$$

This yields the result (3.20a) stated above.

At $O(\varepsilon^{1/3})$, the governing equations (3.32) take the form (3.31), which together with the boundary conditions (3.33) and (3.35c) can be solved using the Wiener–Hopf method. The calculations and explicit solution are given in Appendix A of Moore and Saffman [7], and we do not repeat them here. The result is

$$L_F D_0^F + L_R D_0^R = L D_0^T, \quad (3.37)$$

from which we obtain the matching condition (3.20b) stated above. However, further inspection of the solution reveals that

$$C_1^F - C_1^T = \Delta \frac{L_R}{L} (D_0^R - D_0^F), \quad C_1^R - C_1^T = \Delta \frac{L_F}{L} (D_0^F - D_0^R), \quad (3.38a)$$

$$\text{where} \quad \Delta = -\frac{2\zeta(1/3)}{\pi^{1/3}} (L_F^{1/3} + L_R^{1/3} - L^{1/3}) > 0 \quad (3.38b)$$

and $\zeta(\cdot)$ denotes the Riemann ζ -function. We will use this result to get $O(\varepsilon^{1/3})$ corrections to the leading-order results calculated in §3.2.

At $O(\varepsilon^{2/3})$, the governing equations (3.32) again take the form (3.31b). This can again be solved using the Wiener–Hopf method, but the analysis would be very complicated. Instead, we integrate the analogue of equation (3.31b) over the region $-L_F < X < L_R$, $|\zeta| < M$ for some large constant M . We simplify the resulting left-hand side using the conditions (3.33) and the right-hand side using the conditions (3.35d), and obtain

$$-M \cot \alpha = 2M(L E_0^T + L_F E_0^F + L_R E_0^R) + L D_1^T - L_F D_1^F - L_R D_1^R. \quad (3.39)$$

The terms involving M cancel (by virtue of (3.19)), and we are left with a condition analogous to (3.37).

Thus, the matching conditions (3.20) at $z = h$ can be extended by (3.38, 3.39) to

$$b^F - b^T = 0 + \varepsilon^{1/3} \Delta \frac{L_R}{L} (b_z^R - b_z^F) + O(\varepsilon^{2/3}), \quad (3.40a)$$

$$b^R - b^T = 0 + \varepsilon^{1/3} \Delta \frac{L_F}{L} (b_z^F - b_z^R) + O(\varepsilon^{2/3}), \quad (3.40b)$$

$$L_F b_z^F + L_R b_z^R - L b_z^T = 0 + O(\varepsilon^{2/3}). \quad (3.40c)$$

and we obtain adjusted values of the constants:

$$A_F = \cot \alpha \frac{h^2}{2L(1 + h/H_T)} + \varepsilon^{1/3} \Delta \left[\cot \alpha \frac{h L_R}{2L_F L} - c \frac{h^2}{3L_F} \right] + O(\varepsilon^{2/3}), \quad (3.41a)$$

$$A_R = \cot \alpha \frac{h^2}{2L(1 + h/H_T)} + \varepsilon^{1/3} \Delta \left[-\cot \alpha \frac{h}{2L} + c \frac{h^2}{3L_R} \right] + O(\varepsilon^{2/3}), \quad (3.41b)$$

$$A_T = \cot \alpha \frac{h^2}{2L(1 + h/H_T)} + O(\varepsilon^{2/3}). \quad (3.41c)$$

These can be directly substituted into the solutions (3.19) to yield the corrected results shown in figure 5(a), which do indeed agree better with the numerical results than the leading-order asymptotic results. The corrected force is

$$F = \cot \alpha \frac{h^4}{24L_F} \left(1 + \varepsilon^{1/3} \frac{4\Delta}{h} \right) - c \frac{h^5}{45} \left(\frac{1}{L_F} + \frac{1}{L_R} \right) \left(1 + \varepsilon^{1/3} \frac{5\Delta}{h} \right) + O(\varepsilon^{2/3}), \quad (3.42)$$

and the resulting corrected speed

$$c = \frac{\cot \alpha}{h} \frac{15L_R}{8L} \left(1 - \varepsilon^{1/3} \frac{\Delta}{h} \right) + O(\varepsilon^{2/3}), \quad (3.43)$$

(where Δ is given in (3.38b)) also agrees well with the numerical results (see figure 5(b)).

4 Wedge in a Box with Fixed-buoyancy Walls

We now consider the case when the buoyancy B is prescribed to be equal to the background stratification N^2z on the walls of the bounding box, rather than the walls being insulating with no buoyancy flux through them. We focus on the case when the dimensions of the box and the wedge both have the same scale $O(L_1)$.

We non-dimensionalize lengths using the scale L_1 , stream function using κ , velocity using κ/L_1 , time using L_1^2/κ , and buoyancy perturbation using $\varepsilon N^2 L_1$. The resulting governing equations are

$$b_x = \varepsilon^3 \nabla^4 \psi, \quad \varepsilon (\dot{b} + \psi_x b_z - \psi_z b_x) - \psi_x = \varepsilon \nabla^2 b, \quad (4.1a,b)$$

and the boundary conditions are

$$\psi = \psi_{zz} = 0, \quad b = 0 \quad \text{on symmetry axis} \quad z = 0. \quad (4.2a)$$

$$\psi = \psi_n = 0, \quad b_n = -\frac{1}{\varepsilon} \cos \alpha \quad \text{on wedge front} \quad x = -l + z \cot \alpha, \quad (4.2b)$$

$$\psi = \psi_n = 0, \quad b_n = 0 \quad \text{on wedge rear} \quad x = 0, \quad (4.2c)$$

$$\psi = cz, \quad \psi_x = 0, \quad b = 0 \quad \text{on walls} \quad x = -L_F, L_R, \quad (4.2d)$$

$$\psi = cz, \quad \psi_z = c, \quad b = 0 \quad \text{on ceiling} \quad z = h + H_T. \quad (4.2e)$$

4.1 Numerical results

In this section, we use the parameters

$$\varepsilon = \frac{L_0}{L_1} = \frac{1}{100}, \quad h = H_T = 1, \quad (L_F, L_R) = (2, 1), (2, 2), (2, 3), \quad (4.3)$$

and focus on the particular case $(L_F, L_R) = (2, 1)$ and $\alpha = 45^\circ$. Figure 6 shows numerical results obtained using the finite-element method as described in §3.1.

We again find that a Phillips–Wunsch boundary-layer flow develops on the sloping surface of the wedge, and that there are horizontal boundary layers at $z = 0$ and $z = h$. However, in addition there are also boundary layers on the front and back walls. The buoyancy perturbations remain mainly independent of x as before.

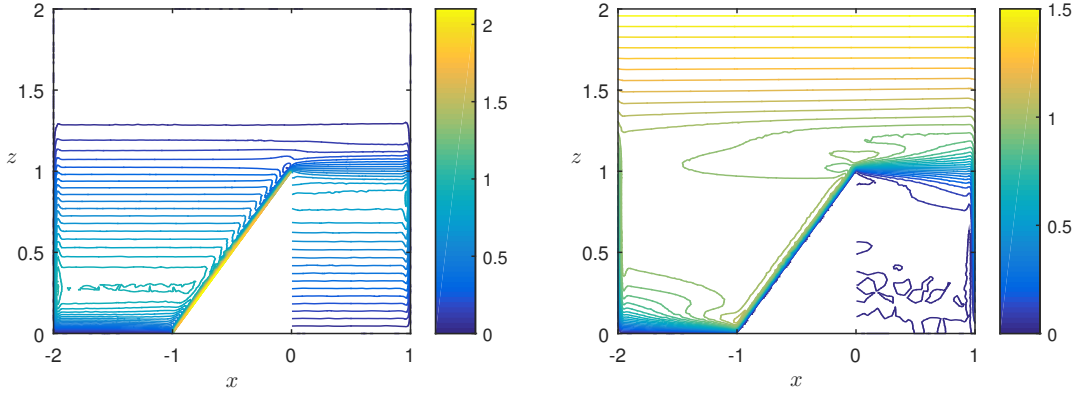


Figure 6: Contour plots of buoyancy perturbation b (left) and stream function ψ (right, flow from left to right in the frame of reference of the wedge) for the parameters (4.3), $(L_F, L_R) = (2, 1)$, $\alpha = 45^\circ$. The contour spacing is 0.05.

4.2 Asymptotic calculation

The asymptotic calculation is again similar to the one in §3.2, although there are more boundary layers involved. The structure of these boundary layers is shown in figure 7, and their relevance will become clear as we proceed with the calculations.

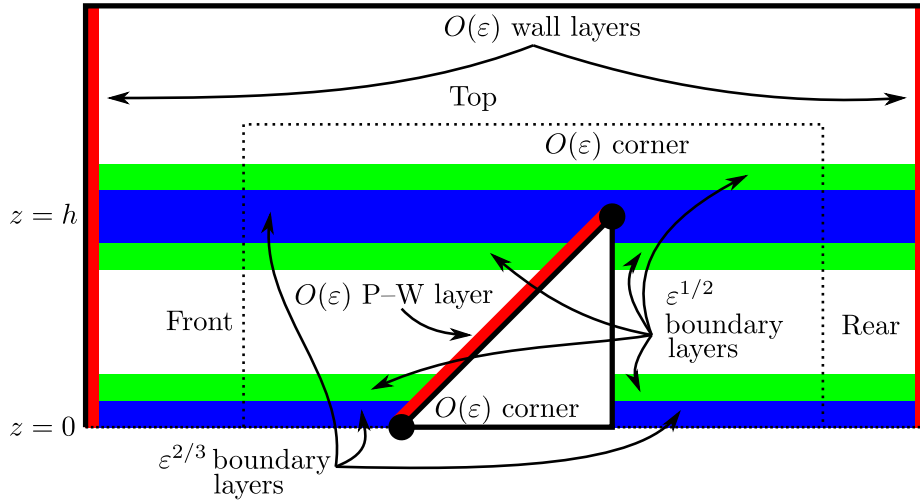


Figure 7: Schematic of asymptotic regions for a wedge in a box with fixed-buoyancy walls. We calculate the force on the dotted box.

4.2.1 Boundary layers on the wedge and walls

We again begin by seeking effective boundary conditions for the outer solutions $\psi^{F,R,T}$ in the x -direction. On the wedge, the calculations from §3.2.1 apply, and we obtain

$$\psi^F = \cot \alpha + O(\varepsilon) \text{ at wedge } x = -l + z \cot \alpha, \quad \psi^R = 0 + O(\varepsilon) \text{ at wedge } x = 0, \quad (4.4)$$

describing how a Phillips–Wunsch flux of magnitude $\cot \alpha$ is driven up the slope.

For the front wall, we obtain a boundary-layer solution analogous to (2.20) by defining a rescaled variable $\xi = (x + L_F(t))/\varepsilon$ and solving the resulting equations

$$b_\xi = \psi_{\xi\xi\xi\xi} + \varepsilon^2 \psi_{\xi\xi z z} + \varepsilon^4 \psi_{z z z z}, \quad \varepsilon^2 \dot{b} + \varepsilon(-cb_\xi + \psi_z b_\xi - \psi_\xi b_x) - \psi_\xi = b_{\xi\xi} + \varepsilon^2 b_{zz}, \quad (4.5a)$$

$$\psi = cz, \quad \psi_\xi = 0, \quad b = 0 \quad \text{at the wall } \xi = 0. \quad (4.5b)$$

The result is

$$\psi = cz + \frac{b_\infty(z)}{\sqrt{2}} \left[1 - \left(\cos \frac{\eta}{\sqrt{2}} + \sin \frac{\eta}{\sqrt{2}} \right) e^{-\eta/\sqrt{2}} \right] + O(\varepsilon), \quad (4.6a)$$

$$b = b_\infty(z) \left[1 - \cos \frac{\eta}{\sqrt{2}} e^{-\eta/\sqrt{2}} \right] + O(\varepsilon). \quad (4.6b)$$

Again, matching the far-field behaviour to the outer solution determines the constant of integration $b_\infty(z)$, and yields an effective condition on the outer stream function in terms of the outer buoyancy

$$\psi^F = cz + \frac{1}{\sqrt{2}} b^F + O(\varepsilon) \quad \text{on the front wall } x = -L_F, \quad (4.7a)$$

A similar analysis of the rear wall yields

$$\psi^R = cz - \frac{1}{\sqrt{2}} b^R + O(\varepsilon) \quad \text{on the rear wall } x = L_R. \quad (4.7b)$$

As for the solution (ψ^T, b^T) in the top region $z \geq h$, we similarly find

$$\psi^T = cz + \frac{1}{\sqrt{2}} b^T + O(\varepsilon) \quad \text{on the front wall } x = -L_F, \quad (4.7c)$$

$$\psi^T = cz - \frac{1}{\sqrt{2}} b^T + O(\varepsilon) \quad \text{on the rear wall } x = L_R. \quad (4.7d)$$

4.2.2 Leading-order outer solution

We now have sufficient information to calculate the leading-order outer solutions. The governing equations (4.1) yield

$$\psi_x^F, b_x^F, \psi_x^R, b_x^R, \psi_x^T, b_x^T = 0 + O(\varepsilon). \quad (4.8)$$

These equations describe, as before, how the flow is too weak to sustain horizontal gradients in buoyancy. In addition, a vertical downwelling is suppressed because the buoyancy perturbation is too weak for its diffusion to balance the resulting advection. Thus, ψ and b are functions of z only and we immediately find, from the effective conditions (4.4, 4.7),

$$\psi^F = \cot \alpha + O(\varepsilon), \quad b^F = \sqrt{2} (\cot \alpha - cz) + O(\varepsilon), \quad (4.9a)$$

$$\psi^R = 0 + O(\varepsilon), \quad b^R = \sqrt{2} cz + O(\varepsilon), \quad (4.9b)$$

$$\psi^T = cz + O(\varepsilon), \quad b^T = 0 + O(\varepsilon). \quad (4.9c)$$

4.2.3 Horizontal $\varepsilon^{1/2}$ boundary layers

We expect, as before, to find boundary layers near $z = 0$ and $z = h$. Assuming that x remains $O(1)$ while z scales with some positive power of ε , two possible balances are found in the governing equations (4.1), corresponding to two boundary-layer thicknesses $\varepsilon^{1/2}$ and $\varepsilon^{2/3}$. These boundary layers are analogous to the outer region (§3.2.2) and $\varepsilon^{1/3}$ boundary layers (§3.4) from the insulating case, respectively. We calculate the solutions for the $\varepsilon^{1/2}$ layer here, while the calculations for the $\varepsilon^{1/3}$ layer are exactly identical to those in §3.4 (apart from a change $X \rightarrow x$ and $\varepsilon \rightarrow \varepsilon^{1/2}$) so we will use those results directly here.

Near $z = 0$, in the front region, we define a rescaled coordinate $\zeta = z/\varepsilon^{1/2}$, and obtain the governing equations

$$b_x^F = 0 + O(\varepsilon), \quad -\psi_x^F = b_{\zeta\zeta}^F + O(\varepsilon^{1/2}), \quad (4.10a,b)$$

whose form we recognize from equation (3.15) for the outer region in the insulating-wall case.

At the left end of this $\varepsilon^{1/2}$ boundary layer, i.e. where it meets the wall, we must seek a corner solution with $x + L_F \sim \varepsilon$ and $z \sim \varepsilon^{1/2}$. The analysis of this region is identical to the wall analysis from §4.2.1, except that the vertical length scale is $O(\varepsilon^{1/2})$ rather than $O(1)$. The resulting effective condition, analogous to (4.7a), is

$$\psi^F = \frac{1}{\sqrt{2}}b + O(\varepsilon^{1/2}) \quad \text{on the front wall } x = -L_F. \quad (4.11a)$$

Similarly, at the right end of the $\varepsilon^{1/2}$ boundary layer, i.e. where it meets the wedge, it is straightforward to verify that the Phillips–Wunsch solution from §3.2.1 is recovered, with result

$$\psi^F = \cot \alpha + O(\varepsilon^{1/2}) \quad \text{on the wedge } x = -l + \varepsilon^{1/2}\zeta \cot \alpha. \quad (4.11b)$$

We proceed, as in §3.2.2, by integrating (4.10b) in x (using the fact that b is independent of x to leading order) and obtain

$$\hat{L}_F b_{\zeta\zeta}^F = \frac{1}{\sqrt{2}}b^F - \cot \alpha + O(\varepsilon^{1/2}), \quad \text{where } \hat{L}_F = L_F - l. \quad (4.12)$$

In matching with the outer layer, i.e. $\zeta \rightarrow \infty$, we require that b does not grow exponentially. At $\zeta = 0$, matching with the $\varepsilon^{2/3}$ layer (cf. §3.4) yields $b^F = 0 + O(\varepsilon^{1/3})$. The solution is

$$b^F = \sqrt{2} \cot \alpha \left[1 - e^{-\zeta/\sqrt{\sqrt{2}\hat{L}_F}} \right] + O(\varepsilon^{1/3}), \quad (4.13a)$$

$$\psi^F = \cot \alpha \left[1 + \frac{x+l}{\hat{L}_F} e^{-\zeta/\sqrt{\sqrt{2}\hat{L}_F}} \right] + O(\varepsilon^{1/3}). \quad (4.13b)$$

Similarly to in §3.4, the nested $O(\varepsilon^{2/3})$ boundary layer ensures that ψ satisfies the condition $\psi = 0$ from (4.2a) on the symmetry axis.

A similar analysis applies near the symmetry axis in the rear region, but in this case the resulting boundary-layer solutions are trivial since the outer solution (4.9b) satisfies the symmetry-axis conditions (4.2a).

Near $z = h$, we instead define the rescaled coordinate $\zeta = (z - h)/\varepsilon^{1/2}$. The rescaled leading-order governing equations (4.10) remain the same, but the conditions (4.4, 4.7) on the wedge and walls become

$$\psi^F = ch + \frac{1}{\sqrt{2}}b^F \quad \text{at } x = -L_F, \quad \psi^F = \cot \alpha \quad \text{at } x = \varepsilon^{1/2}\zeta \cot \alpha, \quad (4.14a)$$

$$\psi^R = 0 \quad \text{at } x = 0, \quad \psi^R = ch - \frac{1}{\sqrt{2}}b^R \quad \text{at } x = L_R, \quad (4.14b)$$

$$\psi^T = ch + \frac{1}{\sqrt{2}}b^T \quad \text{at } x = -L_F, \quad \psi^T = ch - \frac{1}{\sqrt{2}}b^T \quad \text{at } x = L_R, \quad (4.14c)$$

with errors $O(\varepsilon^{1/2})$. Integration of (4.10b) yields

$$L_F b_{\zeta\zeta}^F = \frac{1}{\sqrt{2}}b^F + ch - \cot \alpha + O(\varepsilon^{1/2}), \quad (4.15a)$$

$$L_R b_{\zeta\zeta}^R = \frac{1}{\sqrt{2}}b^R - ch + O(\varepsilon^{1/2}), \quad (4.15b)$$

$$L_A b_{\zeta\zeta}^T = \frac{1}{\sqrt{2}}b^T + O(\varepsilon^{1/2}), \quad (4.15c)$$

where we have defined the average

$$L_A = \frac{L_F + L_R}{2} = \frac{L}{2}. \quad (4.16)$$

Requiring that the solutions b do not grow exponentially in the matching with the outer solutions (i.e. as $\zeta \rightarrow -\infty$ for the front and rear regions and $\zeta \rightarrow +\infty$ for the top region) yields

$$b^F = \sqrt{2} \left[\cot \alpha - ch + A_F e^{\zeta/\sqrt{\sqrt{2}L_F}} \right] + O(\varepsilon^{1/2}), \quad (4.17a)$$

$$b^R = \sqrt{2} \left[ch + A_R e^{\zeta/\sqrt{\sqrt{2}L_R}} \right] + O(\varepsilon^{1/2}), \quad (4.17b)$$

$$b^T = \sqrt{2} \left[A_T e^{-\zeta/\sqrt{\sqrt{2}L_A}} \right] + O(\varepsilon^{1/2}), \quad (4.17c)$$

where the three constants of integration $A_{F,R,T}$ will be determined by matching to the $\varepsilon^{2/3}$ layer. (The corresponding solutions for ψ are easily obtained from (4.10b).)

The nested $\varepsilon^{2/3}$ layer yields the following matching conditions, analogous to (3.40),

$$b^F - b^T = 0 + \varepsilon^{1/6} \Delta \frac{L_R}{L} (b_{\zeta}^R - b_{\zeta}^F) + O(\varepsilon^{1/3}), \quad (4.18a)$$

$$b^R - b^T = 0 + \varepsilon^{1/6} \Delta \frac{L_F}{L} (b_{\zeta}^F - b_{\zeta}^R) + O(\varepsilon^{1/3}), \quad (4.18b)$$

$$L_F b_{\zeta}^F + L_R b_{\zeta}^R - L b_{\zeta}^T = 0 + O(\varepsilon^{1/3}), \quad (4.18c)$$

where Δ is given by (3.38b). Applying these conditions to the solutions (4.17) determines

the constants

$$A_F = \frac{1}{D} \left[-\cot \alpha \left(\sqrt{L_R} + 2\sqrt{L_A} \right) + 2ch \left(\sqrt{L_R} + \sqrt{L_A} \right) \right] + \frac{\varepsilon^{1/6} E}{\sqrt{\sqrt{2}L_F}} \left[\sqrt{L_A} + \sqrt{L_R} \right] + O(\varepsilon^{1/3}), \quad (4.19a)$$

$$A_R = \frac{1}{D} \left[\cot \alpha \sqrt{L_F} - 2ch \left(\sqrt{L_F} + \sqrt{L_A} \right) \right] + \frac{\varepsilon^{1/6} E}{\sqrt{\sqrt{2}L_R}} \left[\sqrt{L_A} + \sqrt{L_F} \right] + O(\varepsilon^{1/3}), \quad (4.19b)$$

$$A_T = \frac{1}{D} \left[-\cot \alpha \sqrt{L_F} + ch \left(\sqrt{L_F} - \sqrt{L_R} \right) \right] + \frac{\varepsilon^{1/6} E}{\sqrt{\sqrt{2}L_A}} \left[\frac{\sqrt{L_R} - \sqrt{L_F}}{2} \right] + O(\varepsilon^{1/3}), \quad (4.19c)$$

where

$$D = 2\sqrt{L_A} + \sqrt{L_F} + \sqrt{L_R}, \quad E = \frac{2\Delta}{D} \left[-\cot \alpha \frac{\sqrt{L_A} + \sqrt{L_R}}{D} + ch \right]. \quad (4.20)$$

We can combine the solutions (4.9, 4.13, 4.17) to form the following composite solutions, which are valid in both the outer regions and the $\varepsilon^{1/2}$ boundary layers:

$$b^F = \sqrt{2} \left[\cot \alpha \left(1 - \exp \frac{-z}{\sqrt{\sqrt{2}\varepsilon\hat{L}_F}} \right) - cz + A_F \exp \frac{-(h-z)}{\sqrt{\sqrt{2}\varepsilon L_F}} \right] + O(\varepsilon^{1/3}), \quad (4.21a)$$

$$b^R = \sqrt{2} \left[cz + A_R \exp \frac{-(h-z)}{\sqrt{\sqrt{2}\varepsilon L_R}} \right] + O(\varepsilon^{1/3}), \quad (4.21b)$$

$$b^T = \sqrt{2} \left[A_T \exp \frac{-(z-h)}{\sqrt{\sqrt{2}\varepsilon L_A}} \right] + O(\varepsilon^{1/3}). \quad (4.21c)$$

4.2.4 Force calculation

As in 3.2.3, the pressure is approximately hydrostatic in the outer regions. Rather than calculating the net force on either the wedge or the bounding box (which are now both lined with boundary layers), we use an intermediate surface (shown in figure 7) which intersects the outer regions away from any boundary layers (apart from the ones at $z = h$ which cannot be avoided). The net force on (the top half of) the wedge is then given by a formula similar to (3.24), and we use the composite solution (4.21) to obtain

$$F = \int_0^h (b^F - b^R)z dz + O(\varepsilon^{5/6}) = \quad (4.22a)$$

$$= \sqrt{2} \left[\cot \alpha \frac{h^2}{2} - \frac{2ch^3}{3} + \varepsilon^{1/2} 2^{1/4} h \left(\sqrt{L_F} A_F - \sqrt{L_R} A_R \right) \right] + O(\varepsilon^{5/6}), \quad (4.22b)$$

where the main error is due to the $O(\varepsilon^{1/3})$ corrections in the $\varepsilon^{1/2}$ layer and the neglect of $O(\varepsilon^{1/6})$ variations in the $\varepsilon^{2/3}$ layer near $z = h$. Hence the speed of the wedge is

$$c(t) = \frac{3 \cot \alpha}{4} \frac{1}{h} \left[1 + \frac{\varepsilon^{1/2} 2^{5/4}}{Dh} \left(\sqrt{L_F L_R} - \frac{1}{2} \sqrt{L_F L_A} + \frac{3}{2} \sqrt{L_R L_A} \right) + \frac{\varepsilon^{2/3} 2 \Delta}{Dh} \left(-\frac{3}{2} \sqrt{L_F} + \frac{1}{2} \sqrt{L_R} - \sqrt{L_A} \right) \right] + O(\varepsilon^{5/6}), \quad (4.23)$$

as this is the value for which $F = 0$.

4.3 Summary and comparison with numerical results

Our analysis of this case with fixed-buoyancy conditions on the bounding walls bears many similarities to the previous analysis with insulating walls (see §3.3). The main difference is the appearance of front and rear outer regions with new behaviour (4.9), namely no leading-order flow ($\psi_x = \psi_z = 0$) relative to the wedge. This phenomenon is called “blocking” and is the stratified analogue of Taylor columns in rotating systems. The Phillips–Wunsch flux up the slope is then not supplied from a uniform downwelling in the front region, but rather from a strong downward current confined to the front wall (and via a symmetry-axis boundary-layer jet).

Near $z = 0$ and $z = h$, there are $\varepsilon^{1/2}$ boundary layers which behave like the outer regions in §3.2.2, and nested inside these are $\varepsilon^{2/3}$ boundary layers which are identical to the $\varepsilon^{1/3}$ layers in §3.4. These two types of boundary layer are the stratified analogues of Stewartson $E^{1/4}$ and $E^{1/3}$ layers for rotating flows.

We compare our composite (outer and $\varepsilon^{1/2}$ -layer) solutions (4.21) with numerical results in figure 8a, and find that they agree well. However, the results for the propulsion speed c are less convincing in the case $\varepsilon = 1/100$ (see figure 8b), and so we have included the case $\varepsilon = 1/400$ as well (figure 8c). In the latter case, we can see a clear improvement between the leading-order result, the $O(\varepsilon^{1/2})$ correction, and finally the $O(\varepsilon^{2/3})$ correction.

5 Wedge in a Very Large or Infinite Domain

Having investigated the cases with a wedge placed in boxes whose size are comparable to or slightly larger than the size of the wedge, we finally consider the case when the box is very much larger than the size of the wedge. We approach this case by considering what happens as the horizontal dimensions of the fixed-buoyancy box in §subsec are increased.

As we can see from e.g. (4.21), the dimensional thickness of the $\varepsilon^{1/2}$ boundary layers is $O((L_0 L)^{1/2})$, while the $\varepsilon^{2/3}$ boundary layers can be seen to have thickness $O((L_0^2 L)^{1/3})$ from e.g. (2.11). As L grows to $O(\varepsilon^{-1} L_1)$, the $\varepsilon^{1/2}$ boundary layers near $z = 0$ and $z = h$ invade and replace the outer region. (Explicit asymptotic solutions can be found in this case, but end up being complicated expressions involving hyperbolic trigonometric functions from the solution of equations similar to (4.15), so we do not report them here.) As L grows further to $O(\varepsilon^{-2})$, the $\varepsilon^{2/3}$ boundary layers fill the domain, and equations like (3.26) need to be solved.

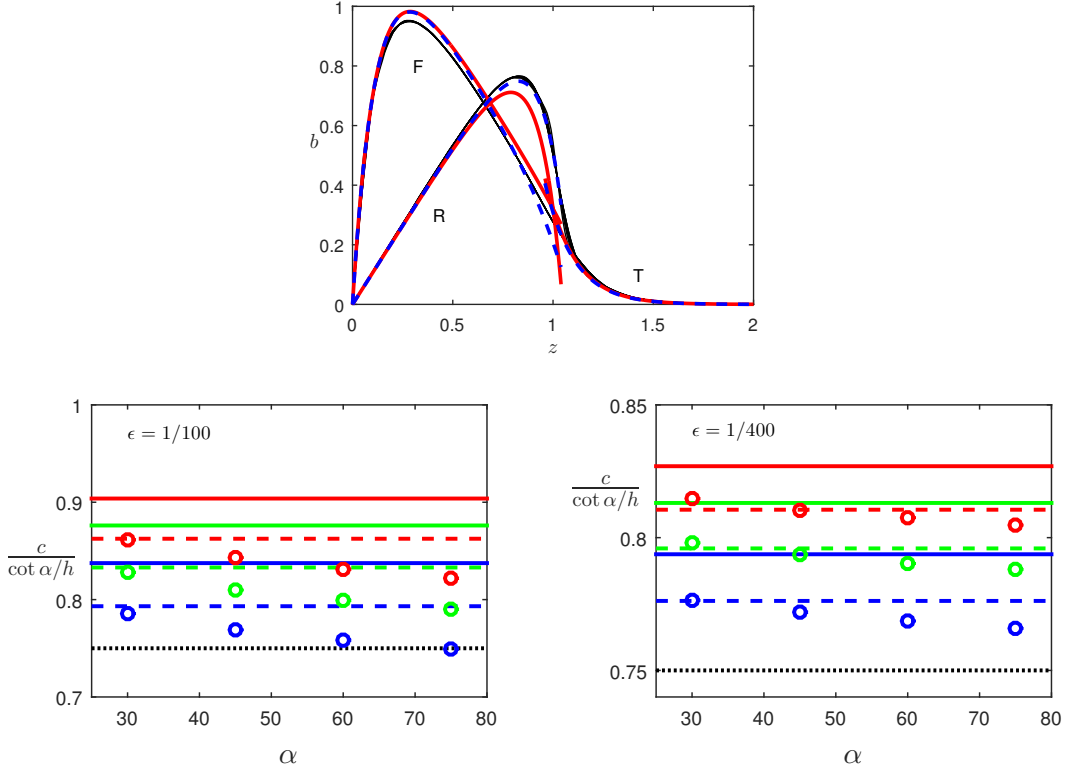


Figure 8: Comparison between asymptotic and numerical results. (a) Buoyancy distribution b as a function of vertical position z for the case shown in figure 6. The thin black curves are numerical data from vertical slices at $-1.9 \leq x \leq -1.1$ and $0.1 \leq x \leq 0.9$ with spacing 0.1 in the forward and rear regions. The thick curves are asymptotic composite solutions (4.21), with the leading-order (solid red curves) or corrected (dashed blue curves) coefficients (4.19, 4.23). (b,c) Propulsion speed c as a function of wedge slope α for the parameters (3.8), showing numerical results (circles) and asymptotic results (4.23) with the leading-order term only (black dotted line), $O(\varepsilon^{1/2})$ corrections (solid lines) and $O(\varepsilon^{2/3})$ corrections (dashed lines). The values of (L_F, L_R) are (2, 3) (top red series), (2, 2) (middle green series) and (2, 1) (bottom blue series).

Finally, for $L \gg \varepsilon^{-2}L_1$ (and $H_T \gg L_1$), we still have to solve the $\varepsilon^{2/3}$ -layer equations, but since the box is much larger than the natural length scales

$$z \sim L_1, \quad x \sim \varepsilon^{-2}L_1, \quad (5.1)$$

we can treat the domain as being infinite, which simplifies the analysis greatly.

5.1 Asymptotic analysis

Based on the scaling (5.1), we non-dimensionalize lengths by L_1 and introduce a stretched horizontal coordinate $X = \varepsilon^2 x$. We scale the stream function by κ , velocity by κ/L_1 , buoyancy by $\varepsilon^2 N^2 L_1$, pressure by $\varepsilon^2 N^2 L_1^2$ and force by $\varepsilon^2 N^2 L_1^3$. We proceed immediately

with calculating the outer solution, valid throughout the domain away from any boundaries. Unlike in §3 and §4, we consider the whole domain rather than just the upper half $z \geq 0$. Also, we work with the stream function $\Psi = \psi - cz$ in the reference frame of the ambient fluid to simplify the decay conditions (but retain the use of a coordinate system moving with the wedge so that the geometry does not evolve with time).

The governing equations (2.9) simplify to

$$b_X = \Psi_{zzzz}, \quad -\Psi_X = b_{zz}, \quad (5.2)$$

with errors of size $O(\varepsilon^2)$ or smaller. As we treat the domain as being infinite, we impose decay conditions in the far field,

$$\Psi, b \rightarrow 0 \quad \text{as} \quad X, z \rightarrow \pm\infty, \quad (5.3a)$$

and the conditions on the bounding box, whether they have fixed buoyancy or no buoyancy flux, have no effect at leading order.

In the horizontally stretched coordinate system, the width of the wedge is $O(\varepsilon^2)$ and hence negligible at leading order. Thus, we can treat it as a cut at $X = 0$, $|z| \leq h$. The Phillips–Wunsch flow on the wedge yields the effective conditions

$$\Psi = \cot \alpha - cz \quad \text{at} \quad X = 0^-, \quad \Psi = -cz \quad \text{at} \quad X = 0^+ \quad \text{for} \quad 0 < z < h \quad (5.3b)$$

on the upper portion of the wedge, and the corresponding antisymmetric conditions ($\Psi = -\cot \alpha + cz$ and $\Psi = cz$) on the lower portion $-h < z < 0$, with errors of size $O(\varepsilon)$.

We exploit the linearity of the leading-order equations (5.2) to decompose the boundary conditions (5.3b), which describe the redistribution of fluid due to Phillips–Wunsch flow, into two parts. The first part, with Ψ anti-symmetric in X ,

$$\Psi = \frac{1}{2} \cot \alpha \quad \text{at} \quad X = 0^-, \quad \Psi = -\frac{1}{2} \cot \alpha \quad \text{at} \quad X = 0^+ \quad \text{for} \quad 0 < z < h, \quad (5.4a)$$

describes the effect of moving fluid from the centreline $z = 0$ to the heights $z = \pm h$, and will be solved by a distribution of sources and sinks on the wedge. However, this gives rise to a pressure distribution that is symmetric in X , and hence yields no net horizontal force. The second part, with Ψ symmetric in X ,

$$\Psi = \frac{1}{2} \cot \alpha - cz \quad \text{at} \quad X = 0^- \text{ and } X = 0^+ \quad \text{for} \quad 0 < z < h, \quad (5.4b)$$

describes the effect of moving fluid from one side of the wedge to the other, and will be solved by a distribution of force singularities on the wedge. The sum of the two solutions form the solution to the original boundary conditions.

Although the point source and point force solutions have been described many times before (see e.g. [5, 7, 3]), we rederive them briefly here for completeness.

5.1.1 Antisymmetric part

We first consider the flow due to a unit point source at the origin. The flow can not be described by a continuous stream function, as it does not satisfy the continuity equation

(2.6b) at the origin (and indeed the conditions (5.4a) are discontinuous on the wedge). However, we can still define

$$\Psi^s(X, z) = \int_0^z u(X, z') dz' \quad \Rightarrow \quad u = \Psi_z^s, \quad (5.5)$$

and the continuity equation (2.6b) with a point source yields

$$u_X + w_z = \delta(X)\delta(z) \quad \Rightarrow \quad w = -\Psi_X^s + \delta(X)\frac{\text{sgn}(z)}{2}, \quad (5.6)$$

where δ is the Dirac δ -function and sgn is the signum function. Including the point source in the governing equations (5.2) and eliminating b yields

$$\Psi_{XX}^s + \Psi_{zzzzz}^s = \delta'(X)\frac{\text{sgn}(z)}{2}. \quad (5.7)$$

We take a Fourier transform in the z -direction and obtain

$$\tilde{\Psi}_{XX}^s = k^6 \tilde{\Psi}^s + \frac{1}{ik} \delta'(X) \quad \Rightarrow \quad \tilde{\Psi}^s = \text{sgn}(X) \frac{1}{2ik} e^{-|k^3 X|}, \quad (5.8)$$

after application of the decay boundary conditions in the X -direction. We only require the solution on the z -axis, so we set $X = 0^\pm$ and invert the Fourier transform to find

$$\Psi^s(0^\pm, z) = \pm \frac{\text{sgn}(z)}{4}. \quad (5.9)$$

Hence, as may be expected, the original antisymmetric conditions (5.4a) are satisfied by the distribution

$$\Psi(X, z) = \cot \alpha [\Psi^s(X, z - h) - 2\Psi^s(X, z) + \Psi^s(X, z + h)] \quad (5.10)$$

of two point sources of strength $\cot \alpha$ at $z = \pm h$ and a point sink of double the strength at $z = 0$.

5.1.2 Symmetric part

We now consider the flow due to a horizontal rightward unit point force at the origin (corresponding to the fluid imparting a unit leftward force on the wedge). This introduces the term $\delta(X)\delta(z)$, on the right-hand side of the approximate horizontal momentum equation $p_X = \Psi_{zzz}$. Modifying the governing equation (5.2) yields

$$\Psi_{XX}^f + \Psi_{zzzzz}^f = -\delta(X)\delta_{zzz}(z). \quad (5.11)$$

As in §5.1.1, it is straightforward to solve the equation using a Fourier transform,

$$\tilde{\Psi}_{XX}^f = k^6 \tilde{\Psi}^f + ik^3 \delta(X) \quad \Rightarrow \quad \tilde{\Psi}^f = -\frac{i \text{sgn}(k)}{2} e^{-|k^3 X|}, \quad (5.12)$$

and inverting the transform at $X = 0$ yields

$$\Psi^f(0, z) = \frac{1}{2\pi z}. \quad (5.13)$$

An unknown force distribution $f(z)$ (symmetric in z) located on the wedge $-h < z < h$ gives rise to the flow

$$\Psi(X, z) = \int_{-h}^h f(z') \Psi^f(X, z - z') dz', \quad (5.14)$$

so the condition (5.4b) yields

$$\frac{1}{2\pi} \int_{-h}^h \frac{f(z')}{z - z'} dz' = \operatorname{sgn}(z) \frac{1}{2} \cot \alpha - cz, \quad (5.15)$$

where the horizontal bar indicates that the Cauchy principal value is taken for the integral. The inversion formula for finite-range Hilbert transforms is given by [14] as

$$g(z) = \frac{1}{2\pi} \int_{-h}^h \frac{f(z')}{z - z'} dz' \quad \Rightarrow \quad \pi \sqrt{h^2 - z^2} f(z) = F - 2 \int_{-h}^h \frac{g(z') \sqrt{h^2 - z'^2}}{z - z'} dz', \quad (5.16)$$

where $F = \int_{-h}^h f(z') dz'$. Hence, consideration of $z = h$ yields the net force as

$$F = 2 \int_{-h}^h \left[\operatorname{sgn}(z) \frac{1}{2} \cot \alpha - cz \right] \frac{\sqrt{h^2 - z^2}}{h - z} dz = 2h \cot \alpha - ch^2 \pi, \quad (5.17a)$$

and the force distribution is given by

$$f(z) = \frac{2}{\pi} \cot \alpha \ln \frac{h + \sqrt{h^2 - z^2}}{|z|} - 2c \sqrt{h^2 - z^2}. \quad (5.17b)$$

The flow field is then determined by (5.14).

As the antisymmetric solution in §5.1.1 has no net force. Hence, we deduce that the net leftward force on the wedge in the original problem is also given by (5.17a), and the propulsion speed is thus

$$c = \frac{2}{\pi} \frac{\cot \alpha}{h} + O(\varepsilon). \quad (5.18)$$

6 Summary and Discussion

We have investigated the two-dimensional diffusion-driven flow that gives rise to propulsion of an insulating wedge in a stably stratified fluid. Using the method of matched asymptotic expansions, we have calculated the flow field, the buoyancy distribution and the propulsion speed in the case when the dimensions of the wedge are much larger than the natural length scale $L_0 = (\kappa \nu / N^2)^{1/4}$ of the flow.

Whether the outer boundaries are insulating (§3), have prescribed buoyancy (§4), or are very far away (§5), we find that the root cause of the propulsion is the Phillips–Wunsch flux of magnitude $\kappa \cot \alpha$ up the sloping upper surface of the wedge (and down the sloping lower surface, by symmetry). This removal of fluid at the apex of the wedge is balanced by vertical flow towards the symmetry axis ahead of the wedge, either throughout the forward region (§3, §5) or along a boundary layer on the front wall (§4). The resulting vertical advection of buoyancy lowers the hydrostatic pressure ahead of the wedge, resulting in a propulsive

force. When the wedge moves at speed c , the $O(ch)$ redistribution of fluid generates a drag force by the same mechanism.

Since the forces on the wedge must balance, we can expect the scaling

$$c \sim \frac{\kappa \cot \alpha}{h} \quad (6.1)$$

to hold. Our calculations confirm this result, with various $O(1)$ numerical prefactors, for all three types of outer boundary condition (3.43, 4.23, 5.18). Somewhat surprisingly, the scaling (6.1) depends on neither the strength N^2 of the background stratification nor the viscosity ν of the fluid. (However, N^2 and ν do affect ϵ and hence the thicknesses of the various boundary layers and the corrections to the leading-order velocity.)

6.1 Comparison with experiments

We compare our theoretical results to the experimental results by Allshouse et al. [1]. In their experiments, the natural length scale was typically $L_0 = O(0.1 \text{ mm})$ while the wedge had size $L_1 \sim h = O(10 \text{ mm})$, so there was indeed a reasonable separation of scales with $\epsilon = L_0/L_1 \ll 1$.

However, since they used wedges whose width-to-length ratio was typically $1/4$ (and never larger than 2), our two-dimensional analysis which requires the wedges to be much wider than they are long does not apply. Also, many of their results are for a wedge with slope $\alpha = 5^\circ$, which is very close to horizontal and again excluded by our analysis. Hence, we can only make a qualitative comparison with their results.

Overall, the experimental results indicate that the velocity c scales with the boundary-layer velocity $c_0 = \kappa \cot \alpha / L_0$, which is $1/\epsilon$ times our scaling (6.1). This is evidenced by figures 3(a,b) in [1], which show that c does depend on the strength of the stratification, closely following the power law $c \propto N^{1/2}$, and that c/c_0 does not vary with the Schmidt number κ/ν . However, we note that the latter figure indicates that the numerical prefactor of the scaling is very small. In addition, the range of velocities in the former figure is limited to $1\text{--}4 \mu\text{m/s}$, so the scaling result is not conclusive. We note that this range is comparable to the values $0.8\text{--}2.5 \mu\text{m/s}$ given by our scaling (6.1). Hence, further study of the three-dimensional case and the near-horizontal case is needed to conclusively decide which scaling is correct.

6.2 Extensions

Our analyses extend relatively easily to two-dimensional objects of other shapes. If the shape of the object is described by $S_-(z) < x < S_+(z)$, then the effective leading-order conditions $\psi = \cot \alpha$ on the wedge slope and $\psi = 0$ on the wedge back are replaced by $\psi = S'_\pm(z)$ at $x = S_\pm(z)$. The variation in slope allows fluid to be entrained or expelled continually along the surface of the object, rather than only at the corners of the wedge, but this is not a problem for the analyses in §3, §4 or §5.

If the object is not top-down symmetric, then the boundary conditions for the stream function will involve an unknown constant corresponding to the unknown circulation around the object. However, this constant is straightforwardly determined by requiring that the

hydrostatic pressure is continuous on both sides of the object. There may also be issues with rotation due to non-zero torque.

A more serious problem with objects of arbitrary shape is that they may have near-horizontal surfaces. In particular, a smooth object which does not have corners at the top and bottom will have horizontal surfaces there. As stated in §2.2, Phillips–Wunsch flow breaks down on surfaces that are too close to horizontal. Whether such top and bottom regions can be ignored for rounded shapes, just like we could ignore the corners of the wedge at a leading order, remains to be seen.

As for extensions into the third dimension, a radically different theoretical approach would be required. This is because we have been relying on calculating the force on the wedge using the hydrostatic pressure, which is only possible due to the two-dimensional wedge acting as a dam between the front and rear regions. When fluid is allowed to flow around the wedge in the third dimension, a large pressure difference between the front and back wedge would simply drive such a flow around the wedge until the pressure force is balanced by viscous drag. Hence, the forces on the wedge are due to both pressure forces and viscous forces at the same order. Thus, it seems that a solution would have to involve solving a complicated equation in a complicated domain.

Nevertheless, based on our two-dimensional analysis we can hypothesize that the three-dimensional system is amenable to simplification by asymptotic decomposition. The Phillips–Wunsch boundary layer would be replaced by a line of sinks at the front of the wedge and two lines of sources at the back, and even though the outer equations have a complicated geometry and require numerical solution the computational cost would be greatly reduced due to the boundary layers not needing to be resolved.

Acknowledgements

I would like to thank Neil Balmforth and Bill Young for proposing this project and for our time together plodding through endless asymptotic expansions on the blackboards.

References

- [1] M. R. ALLSHOUSE, M. F. BARAD, AND T. PEACOCK, *Propulsion generated by diffusion-driven flow*, Nature Physics, 6 (2010), pp. 516–519.
- [2] M. R. FOSTER AND P. G. SAFFMAN, *The drag of a body moving transversely in a confined stratified fluid*, Journal of Fluid Mechanics, 43 (1970), pp. 407–418.
- [3] D. D. FREUND AND R. E. MEYER, *On the mechanism of blocking in a stratified fluid*, Journal of Fluid Mechanics, 54 (1972), pp. 719–744.
- [4] F. HECHT, *New development in freefem++*, Journal of Numerical Mathematics, 20 (2012), pp. 251–265.
- [5] R. C. Y. KOH, *Viscous stratified flow towards a sink*, Journal of Fluid Mechanics, 24 (1966), pp. 555–575.

- [6] D. W. MOORE AND P. G. SAFFMAN, *The rise of a body through a rotating fluid in a container of finite length*, Journal of Fluid Mechanics, 31 (1968), pp. 635–642.
- [7] ———, *The structure of free vertical shear layers in a rotating fluid and the motion produced by a slowly rising body*, Philosophical Transactions of the Royal Society of London A: Mathematical, Physical and Engineering Sciences, 264 (1969), pp. 597–634.
- [8] M. A. PAGE, *Combined diffusion-driven and convective flow in a tilted square container*, Physics of Fluids (1994-present), 23 (2011).
- [9] ———, *Steady diffusion-driven flow in a tilted square container*, The Quarterly Journal of Mechanics and Applied Mathematics, 64 (2011), pp. 319–348.
- [10] M. A. PAGE AND E. R. JOHNSON, *On steady linear diffusion-driven flow*, Journal of Fluid Mechanics, 606 (2008), pp. 433–443.
- [11] ———, *Steady nonlinear diffusion-driven flow*, Journal of Fluid Mechanics, 629 (2009), p. 299.
- [12] T. PEACOCK, R. STOCKER, AND J. M. ARISTOFF, *An experimental investigation of the angular dependence of diffusion-driven flow*, Physics of Fluids (1994-present), 16 (2004), pp. 3503–3505.
- [13] O. M. PHILLIPS, *On flows induced by diffusion in a stably stratified fluid*, Deep Sea Research and Oceanographic Abstracts, 17 (1970), pp. 435–443.
- [14] HEINZ SÖHNGEN, *Die lösungen der integralgleichung $g(x) = (1/2\pi)\int_{-a}^a f(\xi)/(x - \xi) d\xi$ und deren anwendung in der tragflügeltheorie*, Mathematische Zeitschrift, 45 (1939), pp. 245–264.
- [15] G. VERONIS, *Analogous behavior of homogeneous, rotating fluids and stratified, non-rotating fluids*, Tellus, 19 (1967), pp. 326–336.
- [16] ———, *Analogous behavior of rotating and stratified fluids*, Tellus, 19 (1967), pp. 620–634.
- [17] ———, *The analogy between rotating and stratified fluids*, Annual Review of Fluid Mechanics, 2 (1970), pp. 37–66.
- [18] C. WUNSCH, *On oceanic boundary mixing*, Deep Sea Research and Oceanographic Abstracts, 17 (1970), pp. 293–301.